Multiple surface resonance electronic spin states in the strong topological metal Zr_2Te_2P

W. J. Liu,[1,2,*] X. F. Hou,[3,*] H. M. Zha,[1,2] H. J. Qian,[1,2] D. Y. Wang,[1,2] X. P. Shen,[4] M. Ye,[1,2,†] Y. F. Guo,[3,‡] and Shan Qiao[1,2,3,§]

[1]*State Key Laboratory of Functional Materials for Informatics, Shanghai Institute of Microsystem and Information Technology, Chinese Academy of Science, Shanghai 200050, People's Republic of China*

[2]*Center of Materials Science and Optoelectronics Engineering, University of Chinese Academy of Sciences, Beijing 100049, People's Republic of China*

[3]*School of Physical Science and Technology, ShanghaiTech University, Shanghai 201210, People's Republic of China*

[4]*State Key Laboratory of Surface Physics, Department of Physics, Fudan University, Shanghai 200433, People's Republic of China*

(Received 4 September 2022; accepted 5 December 2022; published 28 December 2022)

Nonzero spin polarization occurs in nonmagnetic materials induced by spin-orbital coupling when inversion symmetry is broken. Understanding the origin of spin polarization is essential for finding effective methods of manipulating the electron spin. Recently, nontrivial Dirac node arcs with a novel spin texture have been reported in a tetradymite family M_2Te_2X (with M = Ti, Zr, or Hf and X = P or As) and have potential applications in spintronics. Here, combining spin- and angle-resolved photoemission spectroscopy and first-principles calculations, we have unambiguously distinguished the spin-polarized topological surface states from the bulk continuum states in Zr_2Te_2P, and report that surface resonance Rashba-type spin splittings and spin-momentum-layer locked bulk states exist along with the Dirac node arcs in reciprocal space in adjacent energy ranges. Our work shows the importance of resonance and hybridization between surface and bulk states to their electronic spin textures and provides a platform for developing spintronics devices.

DOI: 10.1103/PhysRevB.106.245144

I. INTRODUCTION

Spin-orbit coupling (SOC) in solid states has been intensively studied for its application in spintronics by manipulating the spin degree of freedom. Spin-related distinctive transport properties such as the quantum spin Hall effect [1–3], quantum anomalous Hall effect [4,5], and new quantum states such as Weyl fermions [6], Ising superconductivity [7,8], chiral topological superconductivity, etc. [9–11], have a huge potential for applications in quantum information, spintronics, and optoelectronics. The study on the spin textures of electronic states and understanding their mechanisms are essential to develop effective strategies for generating substantial spin polarization and manipulating electron spin.

Nonzero spin polarization occurs in nonmagnetic materials induced by SOC when inversion symmetry is broken. The SOC caused by structure inversion asymmetry (SIA) can result in not only spin-polarized surface states [12,13], but also nonzero spin polarization for on-surface bulk continuum, or surface resonance, states [14,15]. The surface Rashba splittings can be tuned via surface doping or an external electric field [16,17]. Local inversion asymmetry (LIA) can induce spin-layer locked states with opposite spin polarizations in inversion counterparts in centrosymmetric crystals while the whole energy bands remain doubly degenerate [18–23]. This spin-layer locking effect is related to the point group of a specific atomic site and is sensitive to the thickness effect [7,19]. Although a system can host spin-polarized states with different origins, it is not easy to distinguish them [15,24,25], and the interplay between SIA and LIA and their effects on the electron spin are still not very clear.

Among the quantum materials with strong SOC, topological materials have drawn much attention because of their nontrivial electronic structure topology [26,27]. Tetradymite-type Bi-based compounds are the earliest discovered three-dimensional topological insulators having massless Dirac fermions with a helical spin texture [28–30]. The topological surface states (TSS) protected by time-reversal (TRS) or specific crystalline symmetry are resistant to defects and impurities on the surface. Recently, nontrivial Dirac node arcs with a novel spin texture have been reported in another tetradymite family M_2Te_2X (with M = Ti, Zr, or Hf and X = P or As) [31]. However, limited by the detection efficiency of a single-channel spin polarimeter, the spin polarizations of TSS and surface resonance bulk states cannot be clearly distinguished from their data. Understanding the origins of spin polarizations is essential for finding effective methods of manipulating electron spin and developing new spintronics devices.

In this paper, we employed spin- and angle-resolved photoemission measurements and first-principles calculations to delve into the electronic spin texture of the strong topological metal Zr_2Te_2P. Owing to the high resolution and efficiency of the multichannel exchange scattering spin polarimeter [25],

*These authors contributed equally to this work.
†yemao@mail.sim.ac.cn
‡guoyf@shanghaitech.edu.cn
§qiaoshan@mail.sim.ac.cn

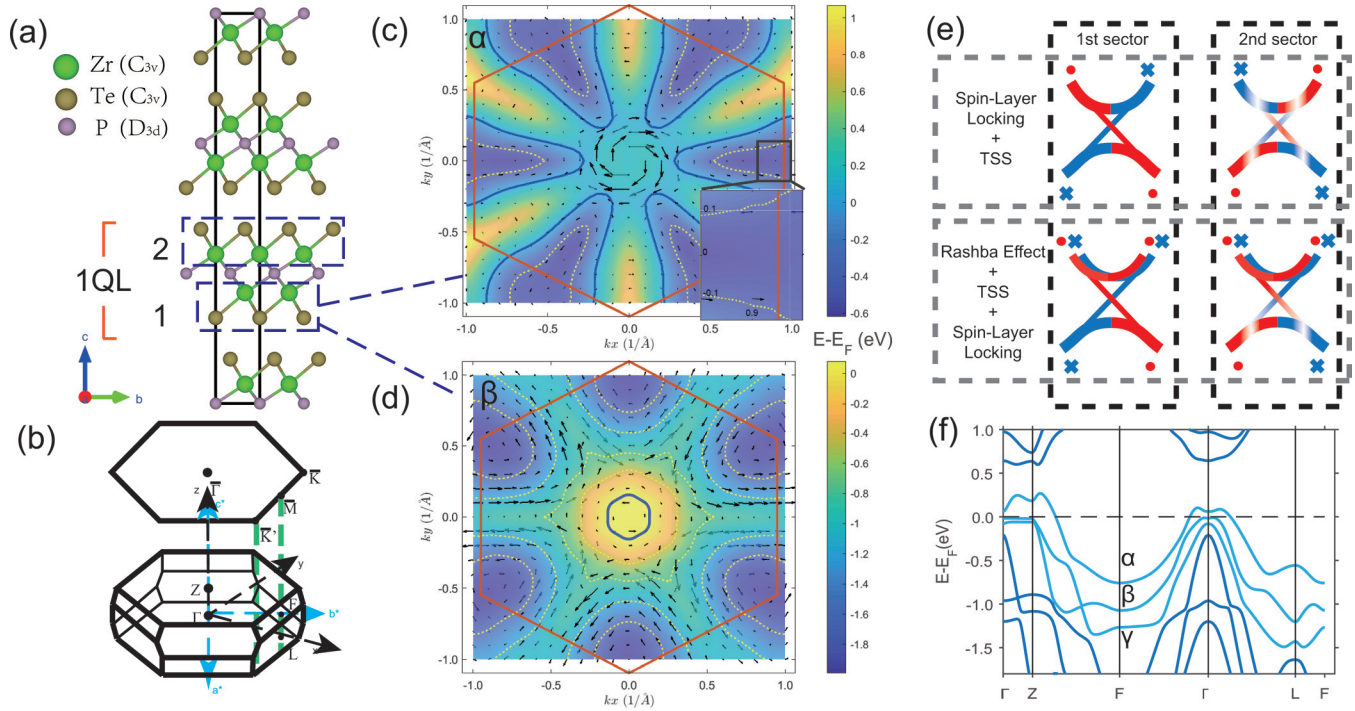

FIG. 1. Crystal structure and electronic states of Zr_2Te_2P. (a) The crystal structure. (b) The three-dimensional (3D) bulk and the projected two-dimensional (2D) surface Brillouin zone. Γ, Z, F, L are the time-reversal-invariant momenta (TRIM). (c) (d) Projected local spin polarization of the lower Zr-Te layer for the α and β bands in (f) at the $k_z = 0$ plane. The black arrow represents the electron spin with its size indicating the magnitude of polarization. Yellow dashed lines indicate the energy contours at $[-0.4, -0.8, -1.2, -1.6]$ eV, and blue lines indicate the Fermi surface. Red hexagons denote the surface Brillouin zone. The inset in (c) is a zoomed picture around the $\bar{M}$ point. (e) Diagram of multiple electronic spin states' hybridization and resonance in one quintuple layer (QL) on the surface. (f) The bulk band structure of Zr_2Te_2P.

the spin-polarized TSS are unambiguously distinguished from the bulk continuum states. The layer-dependent spin polarization, density of states (DOS), and the orbital characters are carefully studied by first-principles calculations to investigate the effect of SIA and LIA on the complicated spin texture of Zr_2Te_2P. Combining the experimental and theoretical results, we prove the coexistence of distinct multiple spin states in Zr_2Te_2P, which are surface resonance Rashba-type spin splittings, TSS, and spin-momentum-layer locked bulk states, and show their interplay on the surface [as illustrated in Fig. 1(e)]. These multiple spin states locate around the $\bar{M}$ point in reciprocal space in adjacent energy ranges, which makes the topological metal Zr_2Te_2P an ideal platform for fundamental and applied research. Furthermore, our work also shows the importance of resonance and hybridization between surface and bulk states to their electronic spin textures.

II. METHODOLOGY

The angle-resolved photoemission spectroscopy (ARPES) and spin-ARPES (SARPES) measurements were performed by a VG Scienta R3000 analyzer integrated with a homemade multichannel very-low-energy diffraction (MCVLEED) spin polarimeter [25] with a He Iα (21.2 eV) light source. The energy and angular resolutions are 12 meV and better than 0.5°, respectively. The samples were cleaved *in situ* and measured at 10^{-8} Pa and 10 K. The geometry of the experimental setup is shown in Fig. 2(a). The density functional theory (DFT) bulk and slab calculations are performed by the Vienna *ab initio* simulation package (VASP) [32] with the Perdew-Burke-Ernzerhof (PBE) [33] method including SOC [34]. The tight-binding method was adopted to study the surface states by using WANNIER90 [35] and WANNIERTOOLS package [36]. Zr_2Te_2P samples were produced using the iodine vapor phase transport method [37]. Careful crystallographic phase and crystal quality examinations were performed on a single-crystal x-ray diffractometer equipped with a Mo $K\alpha$ radioactive source ($\lambda = 0.710\,73$ Å). The diffraction patterns [see Fig. S1 in the Supplemental Material (SM) [38]] could be satisfyingly indexed on the basis of a monoclinic structure with lattice parameters $a = b = 3.81$ Å, $c = 29.18$ Å, and $\alpha = \beta = 90°$, $\gamma = 120°$ in the space group $R\bar{3}m$ (No. 166).

III. RESULTS AND DISCUSSION

The crystal structure [39] is shown in Fig. 1(a). Although the unit cell is centrosymmetric, the point group of both Zr and Te atomic sites is C_{3v} and results in spin-momentum-layer locked bulk states [40]. The Te sites locate beside the van der Waals gaps, and their spin-momentum-layer locking should be stronger. Figures 1(c) and 1(d) show the projected local spin polarizations for bulk bands α and β with $k_z = 0$ of the lower Zr-Te layer [sector one in Fig. 1(a)] in a quintuple layer (their spin textures with $k_z \neq 0$ are shown in Fig. S2 [38]). The spin textures are regulated by C_{3v} symmetry and {110}, {100}, and {010} mirror planes in the conventional unit cell.

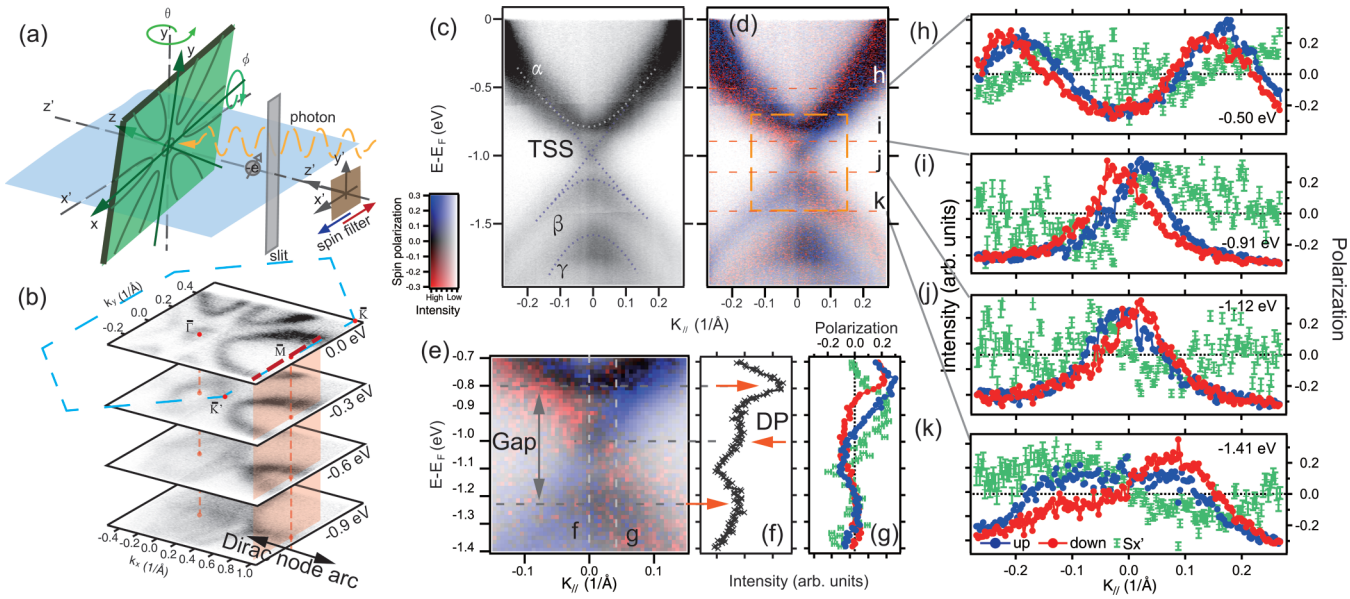

FIG. 2. (a) Geometry setup of SARPES. $Oxyz$ ($Ox'y'z'$) is the laboratory (sample) reference frame. The detected spin polarization is along the x' direction. Up- and down-spin is indicated by the blue and red arrows. (b) Constant energy contours of Zr_2Te_2P at [0.0, −0.3, −0.6, −0.9] eV. The red dashed line and the related pink surface indicate the location of the E-k cut in the Brillouin zone. The Dirac node arc is denoted by the black arrow. (c) Spin-integrated E-k image along $\bar{K}$-$\bar{M}$-$\bar{K}'$. The dotted guideline indicates the bulk band α, β, γ, and the TSS. (d) Spin-polarized E-k image along $\bar{K}$-$\bar{M}$-$\bar{K}'$. Dashed lines (h)–(k) show the locations of the spin-resolved MDCs. (e) Zoomed image of the area in the orange dashed rectangle in (d). (f) The EDC of (e) at $K_\parallel = 0$. The arrows indicate the position of the bottom/top of bulk bands α/β and the Dirac point. (g) The spin-resolved EDC (blue, red) and energy-dependent spin polarization (green) of (e) at $K_\parallel = 0.036$ Å^{-1}. The spectrum weight of the upper Dirac cone (UDC) is much larger than that of the lower Dirac cone (LDC). (h)–(k) Spin-resolved MDCs and momentum-dependent spin polarization at different energies.

There are spin vortices surrounding the $\bar{\Gamma}$ and $\bar{M}$ points for the α band, while the spin vortices are centered at $\bar{K}$ for the β band. In the vicinity of the $\bar{M}$ points, mirror symmetry and TRS rules out the spin components perpendicular to the mirror planes. The α and β bands have opposite spin polarizations around $\bar{M}$. Furthermore, the spin polarizations of the β and α bands are suppressed at $\bar{\Gamma}$ and $\bar{K}$, respectively, which is a consequence of intersector hopping [40,41]. According to Refs. [42,43], the mirror planes also suggest the presence of in-plane TRS, which protects the topological nontrivial Dirac node arcs along $\bar{\Gamma}$-$\bar{M}$. The TSS are located in the gap between the α and β bands with a Z_2 topological quantum number $\nu_0 = 1$ (due to p-d band inversions at L) [44,45]. Interestingly, the spin states in M_2Te_2X could be rather complicated because of the hybridization between TSS and the bulk bands, as discussed in the following.

Figure 2(b) presents the experimental constant energy contours of Zr_2Te_2P. There are six petal-shaped electron pockets along the $\bar{\Gamma}$-$\bar{M}$ directions, which evolve into linear features as the energy decreases, and one hole pocket at the $\bar{\Gamma}$ point. The energy-momentum dispersion along $\bar{K}'$-$\bar{M}$-$\bar{K}$ [Fig. 2(c)] shows Dirac-like surface states with the Dirac point at about −1.0 eV. These features are consistent with previous works [31,44,45] and correspond to topologically nontrivial Dirac node arcs along $\bar{\Gamma}$-$\bar{M}$ in the tetradymite family M_2Te_2X.

The spin-resolved E-k image along $\bar{K}'$-$\bar{M}$-$\bar{K}$ is shown in Fig. 2(d). The direction of spin polarization is parallel to the mirror plane xOz [Fig. 2(a)]. The TSS with linear dispersion are observed in the vicinity of $\bar{M}$ between −0.8 and −1.2 eV. Three peaks in the energy distribution curve (EDC) at $\bar{M}$ [Fig. 2(f)] represent the bottom of the α band, the Dirac point, and the top of the β band. Combining the zoomed image [Fig. 2(e)] and the corresponding spin-resolved momentum distribution curves (MDCs) in Figs. 2(i) and 2(j), the polarization reversal between the left and right branches of the TSS is confirmed. However, the spectrum weight of the upper Dirac cone (UDC) is much larger than that of the lower Dirac cone (LDC) as shown in Fig. 2(g). Below the bulk band gap at −1.4 eV [Fig. 2(k)], the β band merges with the surface states showing a nonzero spin polarization. Even the γ band is spin polarized [Fig. 2(d)] with its spin polarization antiparallel to that of the β band. Interestingly, a spin splitting was found above −0.8 eV where the TSS coexist with the α band, which has not been observed in a previous work [31]. The spin-resolved MDCs [Fig. 2(h)]) clearly show the splitting of up- and down-spin states at −0.5 eV.

In order to exclude the matrix element effect in the photoemission process [46], *ab initio* calculations were carried out. Figures 3(a) and 3(b) show the calculated electronic states and the in-plane spin-polarized electron states in the first QL on the surface along $\bar{K}'$-$\bar{M}$-$\bar{K}$ with the bulk bands indicated by dark cyan regions shown in Fig. 3(a). The mean free path of photoelectrons excited by 21.2 eV photons is about 7 Å, and therefore the spin-resolved spectra [Fig. 2(d)] mainly reflect the electron states in the first QL. From 0 to −0.8 eV, the

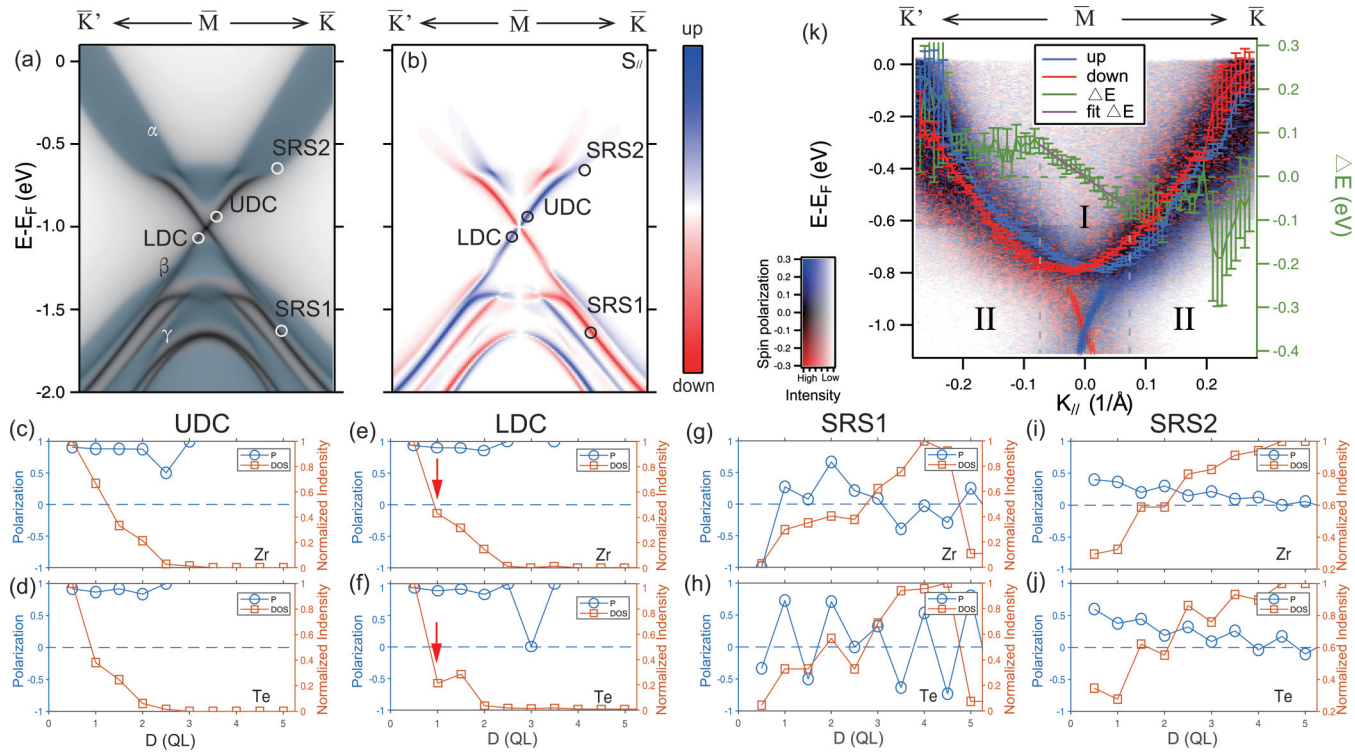

FIG. 3. (a) Calculated electronic states and (b) in-plane spin-polarized electronic states, along $\bar{K}'$-$\bar{M}$-$\bar{K}$ on the surface. The cyan area in (a) indicates the bulk bands. (c)–(j) Layer-dependent average in-plane polarization (blue circle) and normalized density of state (orange rectangle) of Zr and Te atomic layers vs the distance D from the surface, extracted from the ten-layer slab calculations. (c), (d) and (e), (f) corresponding to the upper (UDC) and lower Dirac cones (LDC). (g), (h) and (i), (j) corresponding to the surface resonance states SRS1 and SRS2 indicated by the circle at -0.9, -1.1, -1.6, and -0.7 eV in (a) and (b). The red arrows in (e) and (f) indicate the suppression of DOS in the second sector for LDC. (k) Experimental spin-resolved E-k dispersion along $\bar{K}'$-$\bar{M}$-$\bar{K}$. The blue (red) curve shows the positions of Lorentzian peaks by fitting the spin-resolved EDCs for the α band and MDCs for TSS shown in Fig. 2(d). In region I, ΔE is proportional to $k_\parallel$, and the purple line is the linear fit of $\Delta E(k_\parallel)$, where $\Delta E(k_\parallel) = E_\uparrow(k_\parallel) - E_\downarrow(k_\parallel)$. In region II, ΔE deviates from linear shape as the Dirac node arcs mix with the α band.

calculations coincide with the experimental results that there is a spin splitting of the α band. Below -1.2 eV, the surface states merge with the β band. There are many states around the γ band according to the calculations, which results in a broad structure observed in the experiments. The experimental results match well with the calculations, as they reflect the intrinsic electronic spin states of Zr_2Te_2P. Furthermore, since the M_2Te_2X topological metal family owns the same space group and a similar orbital character [31,45], the spin texture of Zr_2Te_2P is representative and Ti_2Te_2P has a similar spin texture (see Sec. VI in SM [38]).

To go a step further, ten-layer slab calculations were performed to study the variation of polarization and DOS versus the distance from the surface for different (E, k) states [Figs. 3(c)–3(j)]. The TSS marked as UDC and LDC in Figs. 3(a) and 3(b), composed of Zr 4d and Te 5p components, localize mainly in the first QL with their DOS quickly decreasing apart from the surface [Figs. 3(c)–3(f)] and are both fully spin polarized. The DOS of the surface resonance state (SRS1) at -1.60 eV [Figs. 3(g) and 3(h)] extends to the bulk and so does SRS2 at -0.7 eV [Figs. 3(i) and 3(j)]. What is more, the spin polarizations of SRS2 decrease gradually as the distance from the surface increases, showing that the polarization here is mainly caused by SIA. But the polarization of SRS1 related to Te atoms [Fig. 3(f)] changes signs for different Te layers with nondecreasing amplitude, which is a hallmark of spin-layer locking. For SRS2, the spin-layer locking effect of the Te atomic layer can be observed by a slight modulation of local polarization, although being very weak [Fig. 3(j)]. Since the orbital components of electronic states are important to their spin textures [47–49], the different orbital characters of the α and β bands (see Fig. S5 in SM [38]) can explain the competition between the SOCs induced by SIA and LIA here. The β band is dominated by the Te p orbital and the LIA of the Te site results in a spin-layer locked state, whereas the hybridization of Zr d and Te p orbits in the α band attenuates the LIA effect and the α band shows a mainly Rashba character.

The calculations discussed above indicate that the spin splittings observed in the α band originate from the surface Rashba effect. To prove this, the spin-resolved EDCs of bulk bands in Fig. 2(d) above -0.85 eV were fitted by a Lorentzian function and the results are shown in Fig. 3(k). The splitting energy $|\Delta E|$ of up- and down-spin states is indicated with the green line and increases with $K_\parallel$ linearly in the vicinity of $\bar{M}$, which is a hallmark of the Rashba effect. The effective Rashba

coefficient is 1.01 V Å. In region II, the deviation of $\Delta E(k)$ from the linear shape can be attributed to the hybridization between TSS and bulk bands [50–52].

IV. CONCLUSION

So far, we have proved the coexistence of the surface resonance Rashba splittings, TSS, and spin-momentum-layer locked bulk states in Zr_2Te_2P. These electronic spin states could interplay with each other on the surface. As illustrated in Fig. 1(e), in the outmost sector, the spin polarizations of both Rashba splitting and spin-layer-locking states of the α and β bands are the same as those of the Dirac cones near the cross points, whereas in the second sector the spin polarizations of a spin-layer-locking (Rashba splitting) state are opposite (the same) to (as) that of the Dirac cones, which results in an abnormal suppression of the DOS for both LDC [Figs. 3(e) and 3(f)] and bulk states (Figs. S3 and S4 in SM [38]). This also explained the large asymmetry of spectrum weights between UDC and LDC observed in the experiments.

In conclusion, we unambiguously distinguished the spin-polarized TSS from the bulk continuum states and observed the multiple surface resonance electronic spin states in Zr_2Te_2P using SARPES. Combining first-principles calculations, we show how electronic spin textures are determined by the interplay between SIA and LIA and the importance of resonance and hybridization between bulk and surface states. Manipulating electron spin in Zr_2Te_2P and its M_2Te_2X topological metal family, which host these unique surface resonance electronic spin states, via external fields or a proximity effect might bring different spin-related quantum phenomena and have a huge potential in spintronic applications.

ACKNOWLEDGMENTS

This work is supported by National Natural Science Foundation of China (NSFC Grants No. U1632266, No. 11927807, No. U2032207, and No. 92065201) and the National Key R&D Program of China (Grant No. 2017YFA 0305400). Professor Dr. Xiangang Wan and Professor Dr. Qihang Liu are acknowledged for discussions.

[1] B. A. Bernevig, T. L. Hughes, and S.-C. Zhang, Science **314**, 1757 (2006).
[2] C. L. Kane and E. J. Mele, Phys. Rev. Lett. **95**, 226801 (2005).
[3] M. König, S. Wiedmann, C. Brüne, A. Roth, H. Buhmann, L. W. Molenkamp, X.-L. Qi, and S.-C. Zhang, Science **318**, 766 (2007).
[4] R. Yu, W. Zhang, H.-J. Zhang, S.-C. Zhang, X. Dai, and Z. Fang, Science **329**, 61 (2010).
[5] C.-Z. Chang, J. Zhang, X. Feng, J. Shen, Z. Zhang, M. Guo, K. Li, Y. Ou, P. Wei, L.-L. Wang *et al.*, Science **340**, 167 (2013).
[6] N. P. Armitage, E. J. Mele, and A. Vishwanath, Rev. Mod. Phys. **90**, 015001 (2018).
[7] X. Xi, Z. Wang, W. Zhao, J.-H. Park, K. T. Law, H. Berger, L. Forró, J. Shan, and K. F. Mak, Nat. Phys. **12**, 139 (2016).
[8] C. Wang, B. Lian, X. Guo, J. Mao, Z. Zhang, D. Zhang, B.-L. Gu, Y. Xu, and W. Duan, Phys. Rev. Lett. **123**, 126402 (2019).
[9] X.-L. Qi, T. L. Hughes, S. Raghu, and S.-C. Zhang, Phys. Rev. Lett. **102**, 187001 (2009).
[10] P. Zhang, K. Yaji, T. Hashimoto, Y. Ota, T. Kondo, K. Okazaki, Z. Wang, J. Wen, G. D. Gu, H. Ding, and S. Shin, Science **360**, 182 (2018).
[11] S. Nakosai, Y. Tanaka, and N. Nagaosa, Phys. Rev. Lett. **108**, 147003 (2012).
[12] Y. A. Bychkov and E. I. Rashba, JETP Lett. **39**, 78 (1984).
[13] D. Y. Usachov, I. A. Nechaev, G. Poelchen, M. Güttler, E. E. Krasovskii, S. Schulz, A. Generalov, K. Kliemt, A. Kraiker, C. Krellner, K. Kummer, S. Danzenbächer, C. Laubschat, A. P. Weber, J. Sánchez-Barriga, E. V. Chulkov, A. F. Santander-Syro, T. Imai, K. Miyamoto, T. Okuda, and D. V. Vyalikh, Phys. Rev. Lett. **124**, 237202 (2020).
[14] E. E. Krasovskii and E. V. Chulkov, Phys. Rev. B **83**, 155401 (2011).
[15] A. Kimura, E. E. Krasovskii, R. Nishimura, K. Miyamoto, T. Kadono, K. Kanomaru, E. V. Chulkov, G. Bihlmayer, K. Shimada, H. Namatame *et al.*, Phys. Rev. Lett. **105**, 076804 (2010).
[16] M. Bahramy, P. King, A. de la Torre, J. Chang, M. Shi, L. Patthey, G. Balakrishnan, P. Hofmann, R. Arita, N. Nagaosa, and F. Baumberger, Nat. Commun. **3**, 1159 (2012).
[17] P. D. C. King, R. C. Hatch, M. Bianchi, R. Ovsyannikov, C. Lupulescu, G. Landolt, B. Slomski, J. H. Dil, D. Guan, J. L. Mi, E. D. L. Rienks, J. Fink, A. Lindblad, S. Svensson, S. Bao, G. Balakrishnan, B. B. Iversen, J. Osterwalder, W. Eberhardt, F. Baumberger, and P. Hofmann, Phys. Rev. Lett. **107**, 096802 (2011).
[18] K. Gotlieb, C.-Y. Lin, M. Serbyn, W. Zhang, C. L. Smallwood, C. Jozwiak, H. Eisaki, Z. Hussain, A. Vishwanath, and A. Lanzara, Science **362**, 1271 (2018).
[19] L. Bawden, S. P. Cooil, F. Mazzola, J. M. Riley, L. J. Collins-McIntyre, V. Sunko, K. W. B. Hunvik, M. Leandersson, C. M. Polley, T. Balasubramanian, T. K. Kim, M. Hoesch, J. W. Wells, G. Balakrishnan, M. S. Bahramy, and P. D. C. King, Nat. Commun. **7**, 11711 (2016).
[20] T. Xu, B. T. Wang, M. Wang, Q. Jiang, X. P. Shen, B. Gao, M. Ye, and S. Qiao, Phys. Rev. B **100**, 161109(R) (2019).
[21] H. J. Qian, X. Zhang, C. M. Liu, Q. Jiang, W. J. Liu, H. M. Zha, D. Y. Wang, X. P. Shen, M. Ye, Y. F. Guo, and S. Qiao, Phys. Rev. B **104**, 035145 (2021).
[22] X. Zhang, Q. Liu, J.-W. Luo, A. J. Freeman, and A. Zunger, Nat. Phys. **10**, 387 (2014).
[23] J. M. Riley, F. Mazzola, M. Dendzik, M. Michiardi, T. Takayama, L. Bawden, C. Granerød, M. Leandersson, T. Balasubramanian, M. Hoesch *et al.*, Nat. Phys. **10**, 835 (2014).
[24] K. Yaji, A. Visikovskiy, T. Iimori, K. Kuroda, S. Hayashi, T. Kajiwara, S. Tanaka, F. Komori, and S. Shin, Phys. Rev. Lett. **122**, 126403 (2019).
[25] F. Ji, T. Shi, M. Ye, W. Wan, Z. Liu, J. Wang, T. Xu, and S. Qiao, Phys. Rev. Lett. **116**, 177601 (2016).

[26] H. Zhang, C.-X. Liu, X.-L. Qi, X. Dai, Z. Fang, and S.-C. Zhang, Nat. Phys. **5**, 438 (2009).
[27] O. V. Yazyev, J. E. Moore, and S. G. Louie, Phys. Rev. Lett. **105**, 266806 (2010).
[28] X.-L. Qi, Rev. Mod. Phys. **83**, 1057 (2011).
[29] M. Z. Hasan and C. L. Kane, Rev. Mod. Phys. **82**, 3045 (2010).
[30] Y. Zhang, K. He, C.-Z. Chang, C.-L. Song, L.-L. Wang, X. Chen, J.-F. Jia, Z. Fang, X. Dai, W.-Y. Shan *et al.*, Nat. Phys. **6**, 584 (2010).
[31] J. Dai, E. Frantzeskakis, N. Aryal, K.-W. Chen, F. Fortuna, J. E. Rault, P. Le Fèvre, L. Balicas, K. Miyamoto, T. Okuda *et al.*, Phys. Rev. Lett. **126**, 196407 (2021).
[32] G. Kresse and J. Furthmúller, J. Comput. Mater. Sci. **6**, 15 (1996).
[33] J. P. Perdew, K. Burke, and M. Ernzerhof, Phys. Rev. Lett. **77**, 3865 (1996).
[34] D. D. Koelling and B. N. Harmon, J. Phys. C: Solid State Phys. **10**, 3107 (1977).
[35] G. Pizzi, V. Vitale, R. Arita, S. Blügel, F. Freimuth, G. Géranton, M. Gibertini, D. Gresch, C. Johnson, T. Koretsune *et al.*, J. Phys.: Condens. Matter **32**, 165902 (2020).
[36] Q. Wu, S. Zhang, H.-F. Song, M. Troyer, and A. A. Soluyanov, Comput. Phys. Commun. **224**, 405 (2018).
[37] K. Chen, S. Das, D. Rhodes, S. Memaran, T. Besara, T. Siegrist, E. Manousakis, L. Balicas, and R. Baumbach, J. Phys.: Condens. Matter **28**, 14LT01 (2016).
[38] See Supplemental Material at http://link.aps.org/supplemental/10.1103/PhysRevB.106.245144 for details of single crystal growth, spin-resolved ARPES, the first-principles theory calculations, spin-momentum-layer locking, orbital components of the electronic states on surface and the spin texture in other M_2Te_2X components.
[39] K. Tschulik, M. Ruck, M. Binnewies, E. Milke, S. Hoffmann, W. Schnelle, B. P. Fokwa, M. Gilleßen, and P. Schmidt, Eur. J. Inorg. Chem. **2009**, 3102 (2009).
[40] K. Zhang, S. Zhao, Z. Hao, S. Kumar, E. F. Schwier, Y. Zhang, H. Sun, Y. Wang, Y. Hao, X. Ma, C. Liu, L. Wang, X. Wang, K. Miyamoto, T. Okuda, C. Liu, J. Mei, K. Shimada, C. Chen, and Q. Liu, Phys. Rev. Lett. **127**, 126402 (2021).
[41] Y. Zhang, P. Liu, H. Sun, S. Zhao, H. Xu, and Q. Liu, Chin. Rev. Lett. **37**, 087105 (2020).
[42] M. M. Hosen, K. Dimitri, A. K. Nandy, A. Aperis, R. Sankar, G. Dhakal, P. Maldonado, F. Kabir, C. Sims, F. Chou *et al.*, Nat. Commun. **9**, 3002 (2018).
[43] A. Lau, C. Ortix, and J. van den Brink, Phys. Rev. B **91**, 085106 (2015).
[44] H. Ji, I. Pletikosić, Q. D. Gibson, G. Sahasrabudhe, T. Valla, and R. J. Cava, Phys. Rev. B **93**, 045315 (2016).
[45] K.-W. Chen, N. Aryal, J. Dai, D. Graf, S. Zhang, S. Das, P. Le Fèvre, F. Bertran, R. Yukawa, K. Horiba *et al.*, Phys. Rev. B **97**, 165112 (2018).
[46] U. Heinzmann and J. H. Dil, J. Phys.: Condens. Matter **24**, 173001 (2012).
[47] H. Zhang, C.-X. Liu, and S.-C. Zhang, Phys. Rev. Lett. **111**, 066801 (2013).
[48] H. Ishida, Phys. Rev. B **90**, 235422 (2014).
[49] H. Lee and H. J. Choi, Phys. Rev. B **86**, 045437 (2012).
[50] S. Hatta, T. Aruga, Y. Ohtsubo, and H. Okuyama, Phys. Rev. B **80**, 113309 (2009).
[51] M. Ünzelmann, H. Bentmann, P. Eck, T. Kißlinger, B. Geldiyev, J. Rieger, S. Moser, R. C. Vidal, K. Kißner, L. Hammer *et al.*, Phys. Rev. Lett. **124**, 176401 (2020).
[52] H. Ishida, Phys. Rev. B **98**, 205412 (2018).